Electronic structure and optical properties of Sn and SnGe quantum dots

Pairot Moontragoon*, Nenad Vukmirović, Zoran Ikonić, and Paul Harrison

Institute of Microwaves and Photonics,

School of Electronic and Electrical Engineering,

University of Leeds, Leeds LS2 9JT, United Kingdom

Abstract

Self-assembled quantum dots in Si-Ge-Sn system attract research attention as possible direct band gap materials, compatible with Si-based technology, with potential applications in opto-electronics. In this work, the electronic structure near the Γ-point and interband optical matrix elements of strained Sn and SnGe quantum dots in Si or Ge matrix are calculated using the eight-band $\mathbf{k}\cdot\mathbf{p}$ method, and the competing L-valley conduction band states were found by the effective mass method. The strain distribution in the dots was found with the continuum mechanical model. The parameters required for the $\mathbf{k}\cdot\mathbf{p}$ or effective mass calculation for Sn were extracted by fitting to the energy band structure calculated by the nonlocal empirical pseudopotential method (EPM). The calculations show that the self-assembled Sn/Si dots, sized between 4 nm and 12 nm, have indirect interband transition energies between 0.8 to 0.4 eV and direct interband transitions between 2.5 to 2.0 eV. In particular, the actually grown, approximately cylindrical Sn dots in Si with a diameter and height of about 5 nm are calculated to have an indirect transition (to the L valley) of about 0.7 eV, which agrees very well with experimental results. Similar good agreement with experiment was also found for SnGe dots grown on Si. However, neither of these are predicted to be direct band gap materials, in contrast to some earlier expectations.

PACS numbers: 73.21.La, 78.67.Hc, 71.15.Dx

* e-mail: eenpm@leeds.ac.uk

I. INTRODUCTION

The Si-Ge-Sn alloys are considered as an interesting material for future optoelectronic semiconductor devices, despite the difficulties in their growth which stem from the large difference of the lattice constants of the constituents, particularly that of Sn. These alloys are generally compatible with silicon technology and offer many options to engineer the optical properties by using different growth patterns. For example, the devices can be designed based either on layer structures, such as single or multiple quantum wells, or based on nanocluster (quantum dot) structures. The control of their properties can be done by varying the composition of the alloys, such as $Si_{1-x}Ge_x$, $Ge_{1-x}Sn_x$, $Si_{1-x}Sn_x$ and $Ge_{1-x-y}Si_xSn_y$, as described in experimental and theoretical investigations[1–5], which indicated a wide tunability of the band gap of these alloys. For instance, the GeSn alloys can be engineered to cover the wavelength range form 1.5 to 8 μm for interband transitions, and from 8 to 200 μm for conduction- or valence-intersubband transitions[6], indicating a huge potential for optoelectronic applications – as laser diodes, photodetectors, and electro-optical modulators.

Self-assembled Sn quantum dots embedded in Si have been successfully grown in recent years, and it was anticipated that these would also be important nanostructures for optoelectronic devices, because of their potential for synthesis of a Si-based direct bandgap semiconductor, a property not found in the more conventional Ge and SiGe quantum dots. Although bulk Sn is a direct zero band gap semiconductor, the gap at the Γ point is expected to increase, as a combined result of quantum confinement and strain. Growth of Sn/Si dots by temperature modulated molecular beam epitaxy has been reported. A few nanometres thick epitaxially-stabilized metastable Sn_xSi_{1-x} alloy layer with $x = 0.05$ to 0.1 was first grown on Si (001), and then annealed at temperatures between 550 and 800^o C, to form the Sn quantum dots. The process thus differs from the conventional Stranski-Krastanow growth of III/V dots, and is based on a very small equilibrium solubility of Sn in Si (or in Ge), which leads to clusterization of Sn atoms upon annealing the metastable alloy, leaving more or less pure Si around them. Using the Z-contrast cross-sectional high-resolution transmission electron microscopy, the sample was shown to contain dots with diameters in the range of 5-10 nm, located mostly in what was the Sn_xSi_{1-x} alloy layer, and very few in Si spacer layer[7]. The shape of these dots was somewhat irregular, but generally cylindrical or lens-like, rather than the conventional pyramidal. However by the high-resolution

Z-contrast tomography it was found that dots could be in either the cubic α-Sn (zero-gap semiconductor) or the tetragonal β-Sn (metallic) phase[8]. The α-Sn dots transform into the β-Sn phase, more elongated in one direction, when their diameter exceeds a critical value of about 8 nm. In order to investigate optical properties of the Sn-in-Si dots, the luminescence spectrum was measured by using Fourier Transform Infrared Spectroscopy. It was elucidated that the absorption spectrum starts from about 0.3 eV, with the absorption strength of 8×10^3 cm^{-1}, which was believed to be consistent with direct interband transitions[9]. In contrast, the absorption measurements by Karim *et al.*[10] show a relatively weaker broad spectrum at 0.7–1 eV, but no features around 0.3 eV. Similarly, the α-Sn quantum dots embedded in Ge were realized, with a diameter of 32 nm and 10% size distribution. Fitting the simulations to experimental transmittance spectra has lead to a conclusion that direct interband transitions in Sn dots were indeed observed, with an energy gap of 0.45 eV and the absorption coefficient of 3×10^3cm^{-1} near the bandgap edge[11].

On the other hand, theoretical studies of the electronic structure of Sn-based quantum dots, which should help in understanding the features observed in experiments, are missing. In this work, we therefore calculate the single-particle states and interband absoprtion in this type of dots within the framework of envelope function theory. In Sec. II.A and B the theoretical framework is presented. Due to lack of some of material parameters for Sn, these were extracted from empirical nonlocal pseudopotentials, as described in Sec II.C. The results of our study are presented in Sec. III, with special attention devoted to the issue of the nature of the band gap of quantum dot material, which is relevant for optoelectronic devices.

II. COMPUTATIONAL METHOD

In this section we describe the theoretical model used to calculate the electronic structure and optical properties of Sn and SnGe quantum dots. These were assumed to have cylindrical symmetry, being either cylindrical, lens or cone shaped, with diameter (d) and height (h), where $h = d$ was taken for cylindrical, and $h = d/2$ for lens shaped (i.e. hemispherical) dots, while $h = d/2$ and the base angle of 60^o were taken for cone shaped dots, as shown in Fig. 1. Although some papers report tetrakaidecahedron or truncated octahedron shapes[8], the simple cylindrically symmetric shapes should suffice in view of the irregularity present

in all the observed dots.

A. The strain distribution

Due to a large difference in lattice constants of Sn (dots) and the matrix (Si, Ge) there is a considerable strain built in the system, which strongly affects the electronic structure. The strain was described within the continuum mechanical model and calculated by the finite element method, as described in more detail in Ref. 12. The elastic energy of the classical continuum medium is given by

$$W = \frac{1}{2} \sum_{ijkl} \int dV \lambda_{ijkl} \left[e_{ij}(\mathbf{r}) - e_{ij}^{(0)}(\mathbf{r}) \right] \left[e_{kl}(\mathbf{r}) - e_{kl}^{(0)}(\mathbf{r}) \right] \tag{1}$$

where λ_{ijkl} is the elastic tensor relating the stress and strain, $e_{ij}(\mathbf{r})$ are the elastic strain tensor components, and $e_{ij}^{(0)}(\mathbf{r})$ the local intrinsic strain induced by the changes in the lattice constant

$$e_{ij}^{(0)}(\mathbf{r}) = \left(\frac{a\,(\mathbf{r}) - a}{a} \right) \delta_{ij} \tag{2}$$

where $a(\mathbf{r})$ is the unstrained lattice constant at $\mathbf{r}$, and a is the substrate lattice constant. In crystals with the zincblende lattice (we consider only the α-Sn dots) the elastic tensor is of the form

$$\lambda_{ijkl} = C_{12}\delta_{ij}\delta_{kl} + C_{44}\left(\delta_{ik}\delta_{jl} + \delta_{il}\delta_{jk}\right) + C_{an} \sum_{p=1}^{3} \delta_{ip}\delta_{jp}\delta_{kp}\delta_{lp} \tag{3}$$

where C_{12}, C_{44} and $C_{an} = C_{11} - C_{12} - 2C_{44}$ are the elastic constants.

In order to find the strain distribution, the finite element method is used to minimize the total elastic energy. The continuum real space is divided into a nonuniform rectangular grid, and the displacement components are expressed in terms of displacements at grid points, using the first order Lagrange interpolation. The minimization was performed by the conjugate gradient method[13]. The results of strain calculation for cylindrical, lens and cone shaped Sn dots in Si are shown in Fig. 2. The calculated strain field components are used in the eight-band **k·p** calculation, described in the next section.

B. The eight-band k·p model

The Γ-valley electronic structure and interband optical matrix elements of Sn quantum dots were calculated using the eight-band **k·p** method. It describes simultaneously the

conduction band Γ_7^- and the valence bands Γ_8^+ (heavy hole and light hole bands) and Γ_7^+ (spin-orbit split-off band), including the strain dependent coupling and shifts of these bands. In particular, the form given by Bahder[14] was employed. The Hamiltonian is given as $H = H_k + H_s$, where H_s is the strain part and H_k the kinetic part (that also includes the modulated potential $V_0(\mathbf{r})$ and the spin-orbit interaction H_{so}).

The orthonormal wavefunction expansion method was used to find the size-quantized states (eigenenergies and wavefunctions) in a quantum dot. Due to the cylindrical symmetry of the dots considered here, these are taken to be embedded in an outer cylinder of radius R_t and height H_t, with hard walls. Therefore, the envelope function corresponding to band i was written as a linear combination of expansion basis functions

$$\psi_i(\mathbf{r}) = \sum_{nl} A_{inl} f_{nm(i)}(r)\, g_l(z)\, \Phi_m(\phi), \tag{4}$$

where

$$f_{nm}(r) = \frac{\sqrt{2}}{R_t} \frac{J_m(k_{nm} r)}{\left| J_{|m|+1}(k_{nm} R_t) \right|}, \tag{5}$$

$$g_l(z) = \frac{1}{\sqrt{H_t}} \exp\left(i \frac{2\pi l z}{H_t} \right), \tag{6}$$

$$\Phi_m(\phi) = \frac{1}{\sqrt{2\pi}} \exp(im\phi), \tag{7}$$

where l and m are integers and n a positive integer, and J_m is the Bessel function of order m and $k_{nm} R_t$ is its n-th zero. Furthermore, $m(i) = m_f - m_j(i)$, where $m_j(i)$ is the z-component of angular momentum of the Bloch function $|i>$, and quantum number m_f is the z-component of the total angular momentum, which is a good quantum number and is the sum of the angular momentum of the Bloch function and that of the envelope function. The states can therefore be labeled as ne_{m_f} (nh_{m_f}), denoting that an electron (hole) is in the n-th state among the states with the z-component of the total angular momentum m_f.

To find the optical absorption cross section of a transition from an initial state i to a final state f, the interaction Hamiltonian with photons is found from $H' = H\left(\mathbf{k} + \frac{e}{\hbar}\mathbf{A}\right) - H(\mathbf{k})$, where $\mathbf{A} = \varepsilon A$ is the magnetic vector potential, considered constant in space, and where the quadratic terms in $\mathbf{A}$ were neglected, ε is the radiation polarization vector[15]. The optical cross section of the $i \to f$ transition, due to electromagnetic radiation of angular frequency ω is given by[12]

$$\sigma_{if}^{\varepsilon} = \frac{2\pi}{\bar{n}\varepsilon_0 c\omega} |M_{if}|^2\, g(E_f - E_i - \hbar\omega, 2\sigma), \tag{8}$$

where $M_{if} = \langle i \left| H' \right| f \rangle$ is the matrix element which depends on the direction of light polarization, $\bar{n}$ is refractive index, c is speed of light in vacuum, ε_0 is the vacuum dielectric constant, and E_i and E_f are the initial and final state energies, respectively. In order to account for the spread of sizes of self-assembled quantum dots, and various other sources of line broadening, the lineshape function g in Eq. (8) was taken as the Gaussian distribution function, i.e.

$$g\left(E_f - E_i - \hbar\omega, 2\sigma\right) = \frac{1}{\sigma\sqrt{2\pi}} \exp\left[-\frac{(E_f - E_i - \hbar\omega)^2}{2\sigma^2}\right], \tag{9}$$

where σ is the standard deviation of the Gaussian, which typically amounts to 10% of the transition energy for bound-to-bound transitions. The selection rules for the transitions are $|\Delta m| = 0$ for absorption of z-polarized radiation and $|\Delta m| = 1$ for in-plane-polarized radiation.

The **k·p** calculation requires the parameters describing the bulk band structure of the constituent materials. In nonpolar (Si, Ge, Sn) zincblende crystals these are: Luttinger parameters $\gamma_{1,2,3}$, Kane energy E_p, band gap E_g, spin-orbit splitting Δ_{so}, hydrostatic (a_c and a_v), uniaxial (b) and shear (d) deformation potentials, and A' which describes the remote band effects on the conduction band. For Si and Ge all these are well tabulated in the literature, while the data for Sn are more scarce or completely missing. Therefore, the Sn parameters were extracted from the empirical pseudopotential method (EPM), and those of the values which have been reported previously could also be compared against the values obtained here, for improved reliability, as described in the next section.

The highest valence band states in Sn dots (just as in almost all other semiconductors except lead chalcogenides) are derived from the Γ point of the bulk Brillouin zone. If the lowest conduction band state also turns out to be at Γ, the Sn dots would be a direct band gap material. The main 'competitor' to these are the states derived from the conduction band at L point, since it is much lower than the X point in Sn. The eight-band **k·p** method cannot *simultaneously* deliver states at L (a much more elaborate, 30-band **k·p** method[16], or e.g. the pseudopotential calculation[17], would be required for that). In this work, however, we chose to find the L-valley size-quantized states of Sn dots in an approximate manner, using a simple effective mass calculation. For this purpose we use the scalar, angle-averaged effective mass of the ellipsoidal L valleys, and account for the hydrostatic strain only, while ignoring higher order effects, like the intervalley interference[18] etc., which cannot be simply plugged into an effective mass type of calculation. While not of the same level of accuracy

as the $\mathbf{k}\cdot\mathbf{p}$ calculation at Γ, this should still suffice for comparison of direct and indirect gaps in Sn dots. The parameters required were also extracted from the EPM calculation described below.

C. The nonlocal empirical pseudopotential method

The band structure of bulk α-Sn was modelled by the nonlocal empirical pseudopotential method[19]. While requiring some experimental input, this method generally offers a better accuracy for various band structure parameters than does the first-principles density functional theory in the local density approximation without any additional schemes like GW approximation or "scissors correction", as are employed in total energy approaches (see e.g. Ref. 20 for comparison), and it is exactly these band-structure, rather than the ground-state parameters which are of interest in the present work. The electronic structure is found by solving the Schorödinger equation

$$H_{\text{eff}}\psi_{n,\mathbf{k}}\left(\mathbf{r}\right)=\epsilon_{n,\mathbf{k}}\psi_{n,\mathbf{k}}\left(\mathbf{r}\right), \tag{10}$$

in the plane wave basis

$$\psi_{n,\mathbf{k}}\left(\mathbf{r}\right)=\frac{1}{\sqrt{\Omega_0}}e^{i\mathbf{k}\cdot\mathbf{r}}\sum_{\mathbf{G}}a_{n,\mathbf{k}}\left(\mathbf{G}\right)e^{i\mathbf{G}\cdot\mathbf{r}}, \tag{11}$$

where $\mathbf{k}$ is the wave vector in the first Brillouin zone, $\mathbf{G}$ are the reciprocal lattice vectors and Ω_0 is the volume of the primitive cell. The Hamiltonian has local, non-local, and spin-orbit interaction parts:

$$H_{\text{eff}}=H^{loc}+H^{non-loc}+H^{so}. \tag{12}$$

The local part is

$$H^{loc}\left(\mathbf{G}',\mathbf{G}\right)=\frac{\hbar^2}{2m}\left(\mathbf{G}+\mathbf{k}\right)^2\delta_{\mathbf{G},\mathbf{G}'}+V(\mathbf{G}-\mathbf{G}'), \tag{13}$$

where

$$V(\mathbf{G}-\mathbf{G}')=\sum_{\alpha}S_{\alpha}\left(\mathbf{G}-\mathbf{G}'\right)V_{\alpha}\left(\mathbf{G}-\mathbf{G}'\right), \tag{14}$$

and $V_\alpha(\mathbf{G}-\mathbf{G}')$ and $S_\alpha(\mathbf{G}-\mathbf{G}')$ are the pseudopotential form factor and the lattice structure factor of atom type α, respectively.

The nonlocal potential matrix elements relating the basis states with wavevectors $\mathbf{K}$ and $\mathbf{K}'$ are[19]

$$V_\alpha^{NL}(\mathbf{K},\mathbf{K}') = \frac{4\pi}{\Omega_0} A_l(E)(2l+1) P_l(\cos(\theta_{\mathbf{K},\mathbf{K}'})) \times S^i(\mathbf{K}-\mathbf{K}') F_l^i(\mathbf{K},\mathbf{K}'), \quad (15)$$

where

$$F_l(\mathbf{K},\mathbf{K}') = \left\{ \begin{array}{ll} \frac{R_s^3}{2}\left[j_l^2(KR_s) - j_{l-1}(KR_s) j_{l+1}(KR_s)\right], & \mathbf{K}=\mathbf{K}' \\ \frac{R_s^2}{K^2-K'^2}\left[\begin{array}{c} K j_{l+1}(KR_s) j_l(K'R_s) \\ -K' j_{l+1}(K'R_s) j_l(KR_s) \end{array}\right], & \mathbf{K}\neq\mathbf{K}' \end{array} \right\} \quad (16)$$

where $\mathbf{K} = \mathbf{G}+\mathbf{k}$ and $\mathbf{K}' = \mathbf{G}'+\mathbf{k}$, l is the azimuthal quantum number, $\cos(\theta_{\mathbf{K},\mathbf{K}'}) = \mathbf{K}\cdot\mathbf{K}'/|\mathbf{K}\cdot\mathbf{K}'|$, P_l is the Lagrange polynomial of order l , the potential strength A_l is the depth (or height) of the nonlocal square well, R_s is its radius (characterizing the particular atomic type), j_l is the spherical Bessel function of order l, and Ω_0 is the volume of the unit cell. The parameters for Sn given in Ref. 19 were used in this work.

The spin-orbit interaction Hamiltonian, in the plane wave basis, is

$$H^{so}(\mathbf{K}',\mathbf{K}) = -i\lambda\sigma\cdot(\mathbf{K}-\mathbf{K}')\cdot S^i(\mathbf{K}-\mathbf{K}'), \quad (17)$$

where λ is the spin-orbit coupling constant, characterizing the particular atomic type, and σ are the Pauli matrices.

For bulk bandstructure calculations one usually uses the discrete set of local pseudopotential formfactors, at exactly those values of $\mathbf{G}$ which correspond to the equilibrium lattice constant. To extract the deformation potentials, however, one has to consider lattices deformed by uniaxial, shear, or hydrostatic strain, which requires either a continuous local pseudopotential form function $V_\alpha(q)$, or some means of interpolation. The same problem arises in EPM based supercell calculations for superlattices, quantum dots, etc. For Si and Ge, for instance, Friedel et al.[21] have devised such formfunctions, of modified Falicov form

$$V_\alpha(q) = \frac{1}{2}\left(\frac{a_1(q^2-a_2)}{1+e^{(a_3(q^2-a_4))}}\right)\left[\tanh\left(\frac{a_5-q^2}{a_6}\right)+1\right], \quad (18)$$

where q is magnitude of the wavevector, and this form, with improved parameters, has subsequently been employed for various calculations, e.g. Refs. 22,23. We have started with the formfactors for Sn[19], and devised the corresponding formfunction for Sn that reproduces the bandstructure data reported in this and other sources[24–27]. The parameters for Sn, using

a cutoff of 8 Ry, which gives almost full convergence, are given in Table I, along with those for Si and Ge, Ref. 22. The nonlocal and the spin-orbit parts, on the other hand, are already given as continuous functions of the wavevector, and need no further modification for the present purpose.

The band structure of bulk α-Sn along the $L-\Gamma-X$ lines, calculated with these parameters, is given in Fig. 3. Near the Γ-point the EPM bandstructure should coincide with that obtained by the $\mathbf{k}\cdot\mathbf{p}$ method (since it is the second order perturbation theory applied at the Γ point), with appropriately chosen material parameters, and this can be used to extract these parameters[28]. Fitting of the two band structures (including the cases with strain) was performed here by the simulated annealing algorithm[13]. It should be noted that the (almost) *full* congruence can be obtained only in an infinitesimally small vicinity of the Γ-point, while a *very good* congruence can be achieved in a finite range of $\mathbf{k}$ vectors around Γ, say 8–10% of the full span of the Brillouin zone (the range where the $\mathbf{k}\cdot\mathbf{p}$ method is usually considered accurate), and in this work we have targeted the latter choice. The set of parameters for Sn, obtained that way, is given in Table II, together with those for Si and Ge (the later two adopted from Refs. 29,30). Finally, the A' parameter values of Si and Ge were found by using the relation for the conduction band effective mass m^* at the Γ point

$$\frac{\hbar^2}{2m_0}\left(1+A'\right)=\frac{\hbar^2}{2m^*}-\frac{P_0^2}{E_g+\frac{1}{3}\Delta}, \tag{19}$$

where $P_0^2=\hbar^2E_P/2m_0$, and the values of $0.528m_0$ and $0.038m_0$ for Si and Ge, respectively[29].

The Luttinger γ parameters extracted here for Sn, Table II, are considerably different from those given in Ref. 24. However, the effective masses for heavy holes which follow from the two sets are very similar (0.2 in the [001] direction, and 0.55–0.59 in the [111] direction). For light electrons our parameters give the effective masses of 0.018–0.019, and those from Ref. 24 are 0.035–0.039, i.e. differing by a factor of two. However, the experimental values for the latter (Table V in Ref. 24) are around 0.024, which is much closer to our value (not unexpected, since we used a more empirical-related method of band structure calculation). Therefore, we believe that the other parameters for Sn, reported here, are also reasonably reliable. We should also note that the conduction and valence band hydrostatic deformation potentials, a_c and a_v, were individually determined by setting the energy at Γ_8^+ (heavy hole and light hole band) for zero value of the hydrostatic strain, $\epsilon=\epsilon_{xx}+\epsilon_{xx}+\epsilon_{xx}=0$, as the constant reference energy, and then applying strain to find $a_c=\left(\Gamma_7^-\left(\epsilon\right)-\Gamma_7^-\left(\epsilon=0\right)\right)/\epsilon$,

and $a_v = \left(\Gamma_8^+(\epsilon) - \Gamma_8^+(\epsilon = 0)\right)/\epsilon$.

As for the L-valley parameters, the longitudinal (m_l) and transverse (m_t) effective mass are found to be $1.99m_0$ and $0.091m_0$, respectively, in good agreement with other published values $1.35m_0$, $1.48m_0$ and $0.072m_0$, $0.075m_0$, respectively[24,31], and a value of -2.24 eV was extracted for the hydrostatic deformation potential.

The final ingredient required for the $\mathbf{k}\cdot\mathbf{p}$ calculations of heterostructures is the valence band offset at the interface. In the absence of any more reliable experimental data, for Sn grown on $Si_xGe_ySn_{1-x-y}$ we have used an expression in accordance to Jaros[35], i.e. $\Delta V_{v.b.} = 1.17 \cdot x + 0.69 \cdot y$ [eV]. The band energies on the absolute energy scale are not intrinsically contained in the pseudopotential formfactors, and therefore cannot be obtained within the EPM.

III. RESULTS AND DISCUSSION

Using the methods and materials parameters described above, we have investigated the electronic and optical properties of the Sn-based quantum dots, in particular Sn quantum dots embedded in Si[36], and the $Ge_{1-x}Sn_x$ alloy dots. To check the validity of the method we have first done calculations for lens shaped Ge quantum dots in Si, with the diameter and the height of about 100 and 15 nm, respectively. The direct interband transition onset is about 1.3 eV, and the indirect transition (towards the L-point) onset is about 0.72 eV. This is in good agreement with the experimental results of absorption spectrum of the self-assembled Ge/Si quantum dots grown by a solid-source molecular beam epitaxy, in the Stranski-Kranstanov growth mode[37], where a broad peak at 0.7 to 1.0 eV was found.

A. Sn quantum dots

The electronic structure of Sn dots in Si was calculated assuming they were either cylindrical, lens or cone shaped. While the actually grown dots were approximately cylindrical, it is plausible to expect that the other two shapes might be achieved starting with a graded, rather than uniform-composition, Sn-Si alloy layer, which is then annealed. The Sn/Si interface has type-I band alignment, i.e. the Sn dot is the potential well for both electrons and holes at the Γ point. Examples of the wave functions of the lowest (topmost) three states

in the conduction (valence) band at Γ are given in Fig. 4. The direct-transition absorption spectrum of a couple of dot sizes, for the three shapes, is shown in Fig. 5. As expected, the transition energy inversely depends on the dot size, and also depends on the dot shape in the expected manner, being shifted to somewhat higher energies for lens and cone dots. Interestingly, the dot shape determines whether the z-polarized or in-plane-polarized light would be more strongly absorbed.

The main feature from these calculations is that the direct absorption spectrum of Sn/Si dots peaks around 2–2.5 eV. This is larger than the indirect absorption onset in bulk Si (matrix), at about 1.1 eV, but since this absorption is relatively weak one can still expect that these direct transitions might be observed in very thin layers of Si containing Sn dots. It is quite a surprising result that the direct transition energies are so large. This is because of the very large strain in Sn, so large, in fact, that is has converted a zero-gap material into an almost wide-bandgap semiconductor.

However, calculation of L-valley quantized states (the band alignment is here also type-I) shows that these states are much lower in energy than the conduction band states at Γ, as shown in Fig. 6, hence the Sn/Si quantum dots are not a direct gap material. This is a consequence of the fact that the absolute value of L-valey hydrostatic deformation potential is much smaller than that of the Γ valley. Therefore, the effects of strain change the arrangement of Γ and L-valley states. The photoluminescence peak at approx. 0.7 eV, observed in Ref. 10 in Sn dots with the diameter of about 5 nm, agrees very well with the indirect transition energy predicted here, so we believe that it is actually this (indirect and weak) transition that was observed. The likely mechanism for this was the photogeneration of electrons in the X valley of the Si matrix, followed by their capture into lower lying L states of Sn dots, and then by the indirect, phonon-assisted recombination.

B. Sn_xGe_{1-x} quantum dots

Previous studies of Si-Ge-Sn bulk alloys[2–7] show that a direct gap material can be obtained in a suitable range of $Ge_{1-x}Sn_x$ alloy compositions, so we have also calculated the electronic structure of $Ge_{1-x}Sn_x$ quantum dots embedded in Si. Clearly, such dots cannot be grown in Si in the same way as Sn dots are, because Ge is completely soluable in Si, in contrast to Sn. However, growth of $Ge_{1-x}Sn_x$ quantum dots *on* [111] oriented Si substrate, rather than *in* Si

matrix, has been recently reported[38,39]. The dots are approximately hemispherical in shape, they are covered by SiO_2, and are asserted to have a coherent interface with the underlying Si, and are therefore strained. It is less clear, however, what strain conditions apply towards the 'upper' interface with SiO_2, since it even has a different crystalline structure. The strain conditions are important in Sn based dots, as shown above, but are difficult to resolve in the case of $Si/Ge_{1-x}Sn_x/SiO_2$ dots. Furthermore, the different crystalline structures of Sn and SiO_2 would discourage one to use the $\mathbf{k}\cdot\mathbf{p}$ method at all, but the fact that the band discontinuities between Sn and SiO_2 are very large effectively makes it irrelevant what is on the other side of Sn, and the $\mathbf{k}\cdot\mathbf{p}$ method can still be used to a good accuracy. Overall, we expect that the calculation for $Ge_{1-x}Sn_x$ quantum dots fully embedded in Si, with their axis in the [001] direction, as was performed in this work, is an approximate description of the actual structure.

In these calculations the Luttinger parameters, deformation potentials and the spin-orbit splitting of $Ge_{1-x}Sn_x$ were estimated using Vegard's law, while the direct band gap and lattice constant were calculated by using the quadratic interpolation, with bowing parameters of 2.49 eV[2,4,40] and 0.166 Å[41], respectively. The results for the dot sizes between 4 and 12 nm, and for different compositions $0 \leq x \leq 1$, show that the indirect interband transitions (towards the L valley states) occur from 0.8 to 0.4 eV, while the direct interband transition occur from 2.5 to 1.5 eV, as also shown in Fig. 6(b), implying that they are indirect gap materials. The direct energy band gap depends quadratically on the Sn composition (note the non-monotonic dependence of E_g on x in Fig. 6(b)), because the bowing parameter in the direct band gap of the alloy has a strong influence. Experimentally, for dots of small diameters (<10 nm) the absorption peaks between 1.5 eV and 2 eV were found[38], which agrees very well (perhaps surprisingly so, in view of the approximations involved) with the data for direct transitions given in Fig. 6(b). Nevertheless, these dots are (predicted to be) an indirect band gap material.

Finally, we have also made calculations for Sn dots embedded in Ge, which can be fabricated in the same manner as Sn/Si dots, due to the small solubility of Sn in Ge. Here we find the type-II alignment (after the strain), i.e. the dot is the potential well only for holes, but not for either Γ or L-valley electrons. The conduction band edge at L is well below that at Γ inside the Sn dot, since it is largely determined by strain, and this does not change too much when going from Si to Ge matrix. This in turn implies that Sn dots in a Si_xGe_{1-x}

matrix (which presumably could also be grown by the same technique) cannot become a prominent direct gap material for any value of x.

IV. CONCLUSION

Using the nonlocal empirical pseudopotential method to extract the $\mathbf{k}\cdot\mathbf{p}$ parameters and deformation potentials of bulk Sn, and the 8×8 $\mathbf{k}\cdot\mathbf{p}$ method to calculate the electronic structure and optical properties of quantum dots, we have explored the properties of self-assembled Sn dots embedded in Si, and $Ge_{1-x}Sn_x$ quantum dots in Si or in Ge, relevant for optoelectronic applications. Cylindrical, lens and truncated cone shaped dots were considered. The self-assembled Sn/Si dots of size between 4 nm and 12 nm were found to have indirect interband transitions (towards the L-valley size-quantized states) from 0.8 to 0.4 eV, and direct interband transitions from 2.5 to 2.0 eV. The indirect interband transition energies compare very well with the experimental reported absorption peaks[10]. However, the indirect nature of the lowest interband transition makes Sn or SnGe quantum dots in Si matrix the unlikely candidates for optoelectronic devices, except perhaps for pure absorption applications, in contrast to some previous expectations.

[1] G. Sun, H. H. Cheng, J. Menendez, J. B. Khurgin, and R. A. Soref, Appl. Phys. Lett. **90**, 11992 (1990).

[2] G. He, and H. A. Atwater, Phys. Rev. Lett. **79**, 1937 (1997).

[3] M. Bauer, J. Taraci, J. Tolle, A. V. G. Chizmeshya, S. Zollner, D. J. Smith, J. Menendez, C. Hu, and J. Kouvetakis, Appl. Phys. Lett. **81**, 2992 (2002).

[4] P. Moontragoon, Z. Ikonić, and P. Harrison, Semicond. Sci. Technol. **22**, 742 (2007).

[5] J. Kouvetakis, J. Menéndez, and A. G. V. Chizmeshya, Annual Review of Materials Research **36**, 497 (2006).

[6] J. Kouvetakis, and A. G. V. Chizmeshya, J. Mater. Chem. **17**, 1649 (2007).

[7] Y. Lei, P. Mock, T. Topuria, N. D. Browning, R. Ragan, K. S. Min, and H. A. Atwater, Appl. Phys. Lett. **82**, 4262 (2003).

[8] I. Arslan, T. J. V. Yates, N. D. Browning, and P. A. Midgley, Science **309**, 2195 (2005).

[9] R. Ragan, K. S. Min, and H. A. Atwater, Materials Science and Engineering B **87**, 204 (2001).

[10] A. Karim, G.V. Hansson, W.-X. Ni, P.O. Holtz, M. Larsson and H.A. Atwater, Optical Materials **27**, 836 (2005).

[11] R. Ragan, Ph.D. dissertation, California Institute of Technology, 2002.

[12] N. Vukmirović, Ž. Gačević, Z. Ikonić, D. Indjin, P. Harrison, and V. Milanović, Semicond. Sci. Technol. **21**, 1098 (2006).

[13] W. H. Press, S. A. Teukolsky, W. T. Vetterling, and B. P. Flannery *Numerical Recipes in Fortran 77* (Cambridge University Press, Cambridge, 1992).

[14] T. B. Bahder, Phys. Rev. B **41**, 11992 (1990).

[15] Z. Ikonić, V. Milanović, and M. Tadić, J. Phys.: Condens. Matter **7**, 7045 (1995).

[16] S. Richard, F. Aniel, and G. Fishman, Phys. Rev. B **70**, 235204 (2004).

[17] L. W. Wang, A. Franceschetti, and A. Zunger, Phys. Rev. Lett. **78**, 2819 (1997).

[18] D. Ahn, J. Appl. Phys. **98**, 033709 (2005).

[19] J. R. Chelikowsky, and M. L. Cohen, Phys. Rev. B **14**, 556 (1976).

[20] H. Lopez, A. N. Chantis, J. Sune, and X. Cartoixa, J. Computational Electronics **6**, 195 (2007).

[21] P. Friedel, M. S. Hybertsen, and M. Schlüter, Phys. Rev. B **39**, 7974 (1989).

[22] M. V. Fischetti, and S. E. Laux, J. Appl. Phys. **80**, 2234 (1996).

[23] P. Yu, J. Wu, and B. F. Zhu, Phys. Rev. B **73**, 235328 (2006).

[24] T. Brudevoll, D. S. Citrin, M. Cardona, and N. E. Cristensen, Phys. Rev. B **48**, 8629 (1993).

[25] S. Adachi, J. Appl. Phys. **66**, 813 (1989).

[26] H. U. Middelmann, L. Sorba, V. Hinkel, and K. Horn, angle-resolved photoemission", Phys. Rev. B **35**, 718 (1987).

[27] G. P. Srivastava, J. Phys. C: Solid State Phys. **16**, 1649 (1983).

[28] D. J. Dugdale, S. Brand, and R. A. Abram, Phys. Rev. B **61**, 12933 (2000).

[29] S. Ridene, K. Boujdaria, H. Bouchriha, and G. Fishman, Phys. Rev. B **64**, 085329 (2001).

[30] C. G. Van de Walle, Phys. Rev. B **39**, 1871 (1989).

[31] M. Cardona, and F. H. Pollak, Phys. Rev. **142**, 530 (1966).

[32] P. Lawaetz, Phys. Rev. B **4**, 3460 (1971).

[33] B. L. Booth, and A. W. Ewald, Phys. Rev. **168**, 805 (1968).

[34] B. J. Roman, and A. W. Ewald, Phys. Rev. B **5**, 3914 (1972).

[35] M. Jaros, Phys. Rev. B **37**, 7112 (1988).

[36] P. Mock, Y. Lei, T. Topuria, N. D. Browning, R. Ragan, K. S. Min, and H. A. Atwater Physical Chemistry of Interfaces and Nanomaterials **4807**, 71 (2002).

[37] Z. Yang, Y. Shi, J. Liu, B. Yan, R. Zhang, Y. Zheng, and K. Wang Materials Letters **58**, 3765 (2004).

[38] Y. Nakamura, A. Masada, and M. Ichikawa, Appl. Phys. Lett. **91**, 013109 (2007).

[39] Y. Nakayama, K. Takase, T. Hirahara, S. Hasegawa, T. Okuda, A. Harasawa, I. Matsuda, Y. Nakamura, and M. Ichikawa, Japan. J. Appl. Phys. **46**, L1176 (2007).

[40] V. R. D'Costa, C. S. Cook, A. G. Birdwell, C. L. Littler, M. Canonico, S. Zollner, J. Kouvetakis, and J. Menéndez, Phys. Rev. B **73**, 125207 (2006).

[41] P. Aella, C. Cook, J. Tolle, S. Zollner, A. V. G. Chizmeshya, and J. Kouvetakis, Appl. Phys. Lett. **84**, 888 (2004).

Parameters	a_1	a_2	a_3	a_4	a_5	a_6
Si	0.1299	3.469	0.7618	3.574	5.0	0.3
Ge	0.2962	2.527	0.6813	1.159	5.0	0.3
Sn	0.1221	2.145	3.100	2.741	5.0	0.3

TABLE I: Parameters of the pseudopotential of α-Sn (this work), and for Si and Ge, Ref. 22. The normalization (lattice) volumes for Si, Ge, and Sn are 134.3, 151.8, and 230.5 a.u., respectively.

	Value(unit)			
Parameter	Sn (this work)	Sn (other sources)	Si	Ge
γ_1	-25.19	-12.0[a],-14.97[b],-19.2[c]	4.285	13.38
γ_2	-15.11	-8.45[a],-10.61[b],-13.2[c]	0.339	4.24
γ_3	-13.53	-6.84[a],-8.52[b],-9.0[c]	1.446	5.69
E_p	14.26 eV	23.8[b] eV	21.60 eV	26.30 eV
A'	-3.25		-4.285	-7.519
a_c	-8.714 eV	$a_c + a_v$=-7.04[a]	1.98 eV	-8.24 eV
a_v	1.62 eV		2.46 eV	1.24 eV
b	-2.01 eV	-2.3[d]	-2.1 eV	-2.9 eV
d	-0.39 eV	-4.1[d]	-4.8 eV	-5.3 eV
Δ	0.70 eV	0.72[a],0.77[b] eV	0.044 eV	0.29 eV
E_g	-0.408 eV	-0.406[a]-0.413[b] eV	4.185 eV	0.898 eV

TABLE II: The $\mathbf{k}\cdot\mathbf{p}$ and deformation potential parameters for bulk α-Sn, Si and Ge. (*a*) – Ref. 24, *b*) – Ref. 32, *c*) – Ref. 33, *d*) – Ref. 34.)

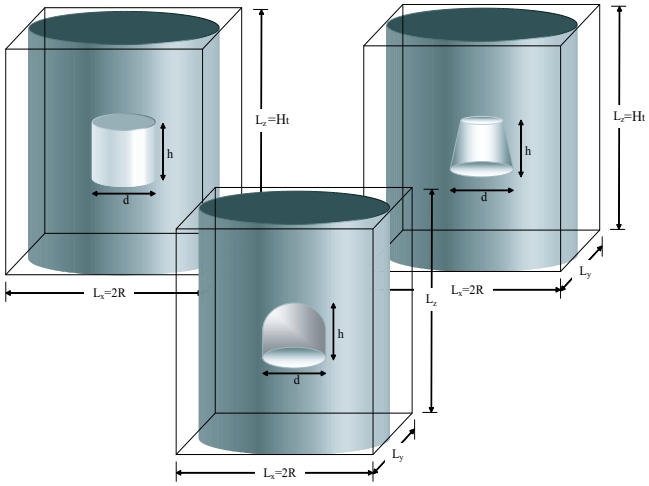

FIG. 1: Cylindrical, lens and cone shaped quantum dots.

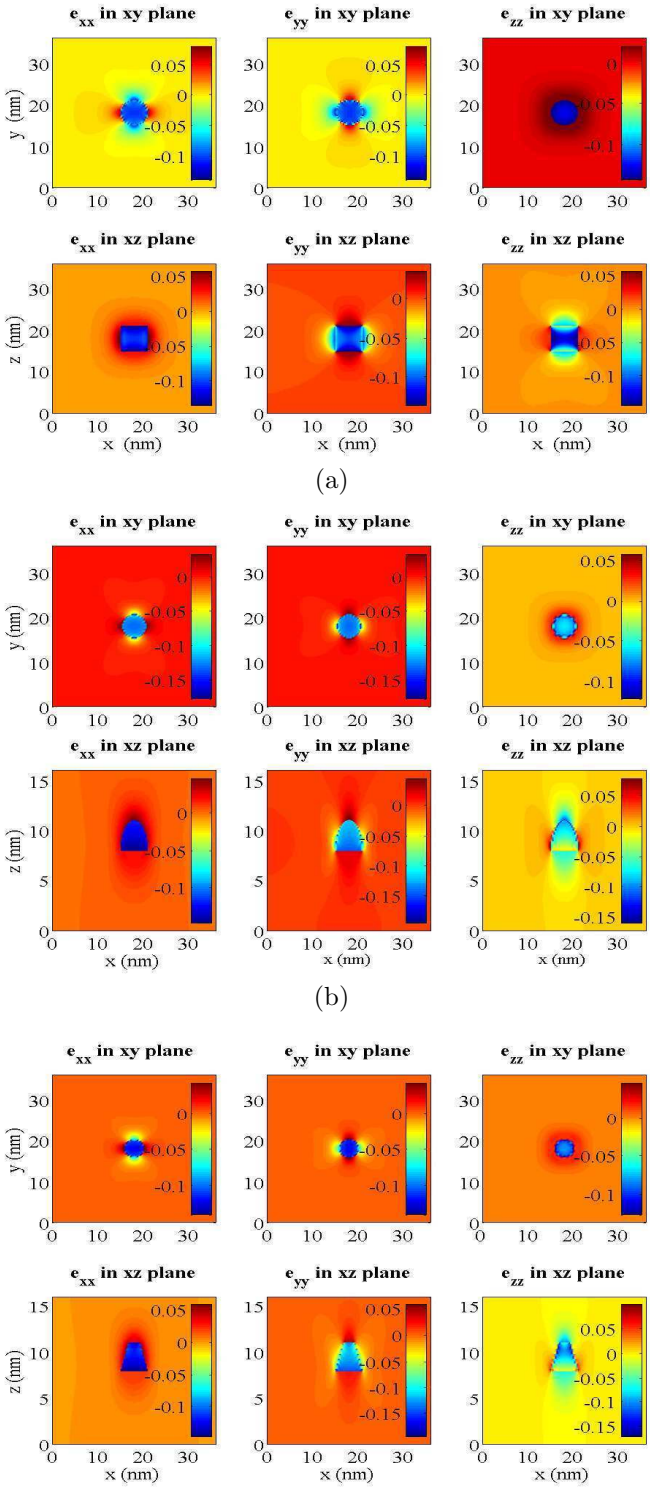

FIG. 2: Strain distribution in (a) cylindrical, (b) lens, and (c) cone shaped Sn quantum dots in Si matrix.

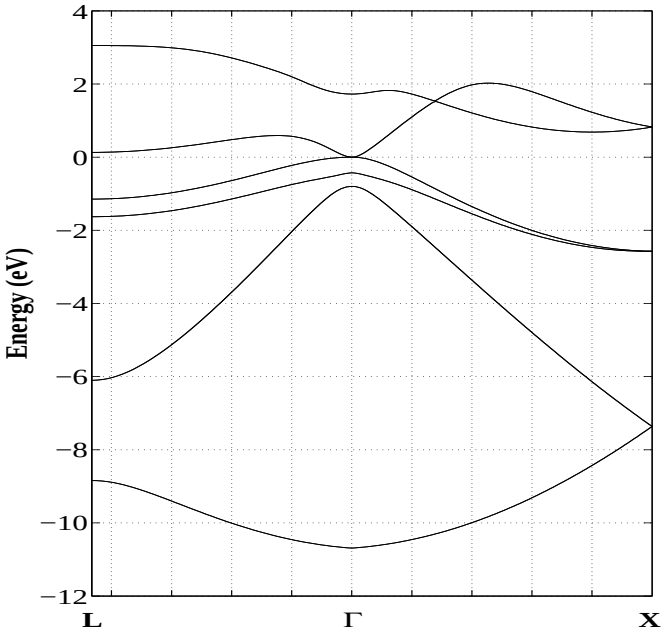

(a)

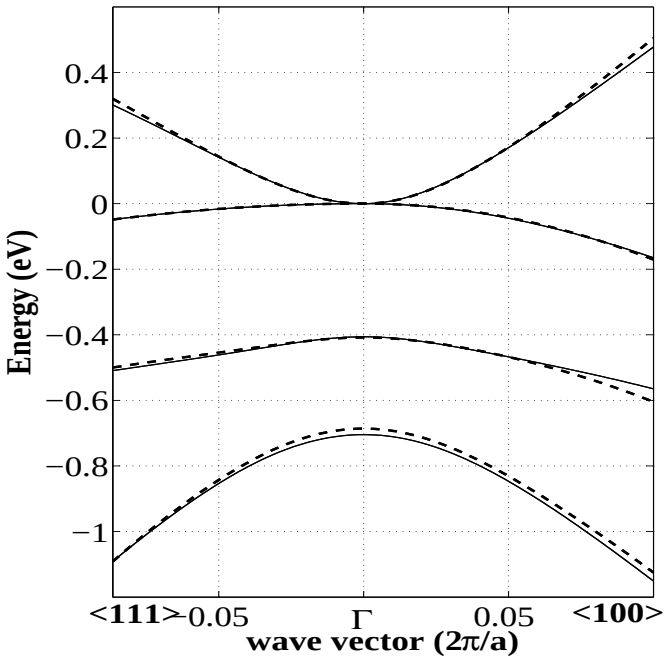

(b)

FIG. 3: a) The EPM calculated band structure of bulk α-Sn, and (b) the band structure near the Γ point, calculated by the eight-band $\mathbf{k}\cdot\mathbf{p}$ method with the obtained parameters (dashed), compared to the band structure calculated by EPM (solid lines).

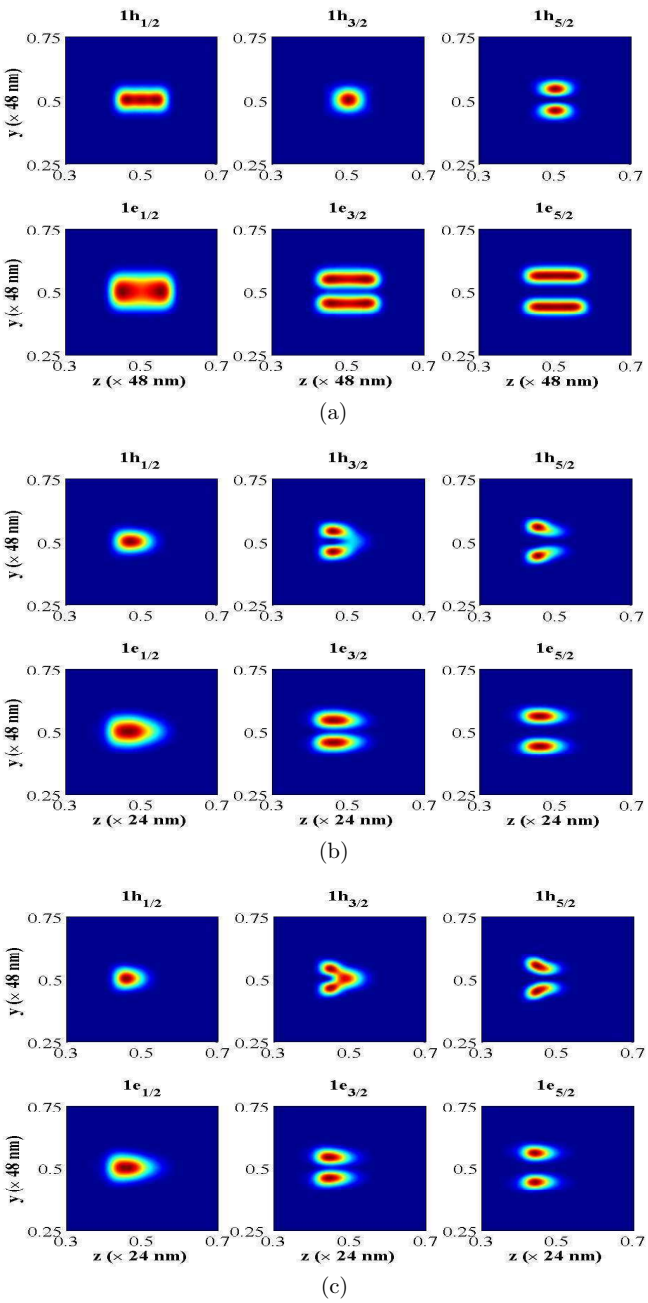

FIG. 4: The wave functions of a couple of conduction and valence quantized states in 8 nm diameter Sn/Si quantum dots of (a) cylindrical, (b) lens, and (c) cone shape.

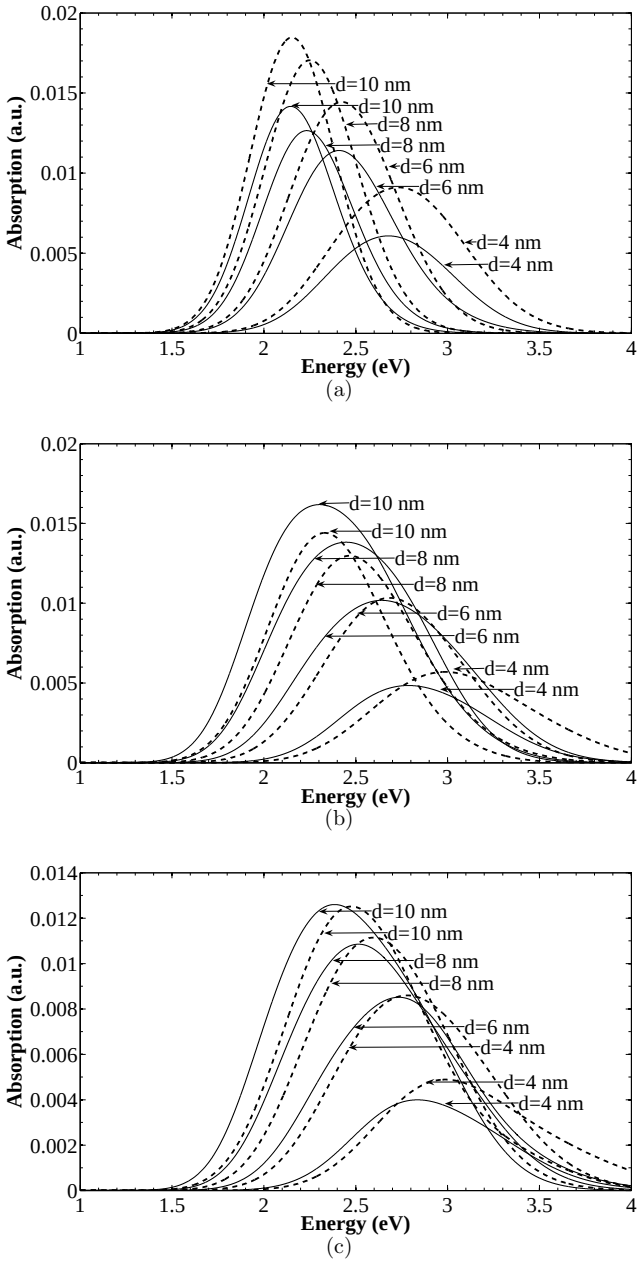

FIG. 5: The direct interband absorbtion spectra of Sn/Si quantum dots of (a) cylindrical, (b) lens, and (c) cone shape, for different dot diameters d. Solid lines correspond to z-polarized light (along the dot axis), and dashed lines to in-plane polarized light.

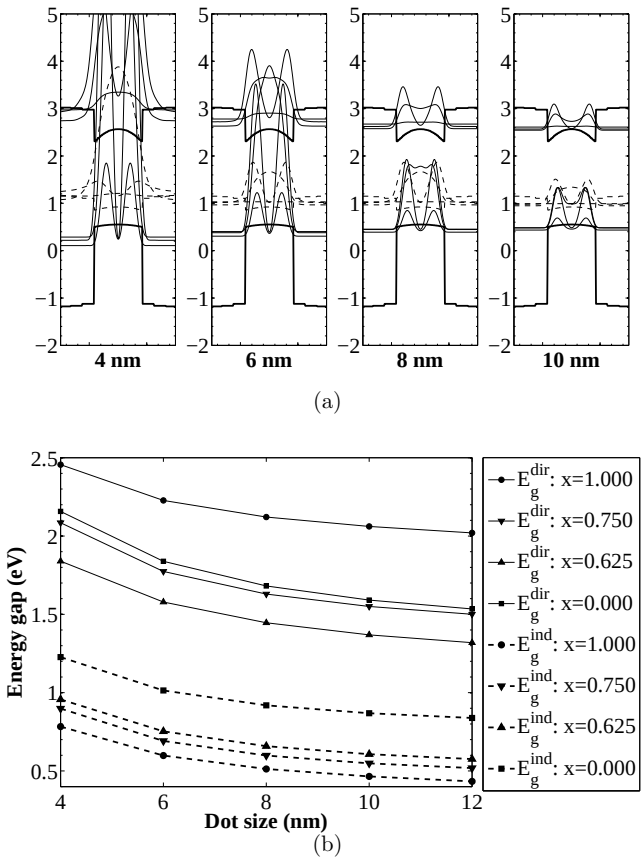

FIG. 6: (a) The wavefunctions squared along the axis of Sn/Si dots with diameters from 4 to 10 nm, for the quantized states at Γ (solid) and at L point (dashed); (b) The dependence of the band gap of $Ge_{1-x}Sn_x$/Si dots on the diameter and composition x.